Orientation Dependence of Charge-Transfer Processes on TiO_2 (Anatase) Single Crystals

Roland Hengerer[a], Ladislav Kavan[a,b], Petr Krtil[b] and Michael Grätzel[a]

[a]*Laboratory of Photonics and Interfaces, Swiss Federal Institute of Technology, Ecublens, CH-1015, Lausanne, Switzerland*

[b]*J. Heyrovsky Institute of Physical Chemistry, Academy of Sciences of the Czech Republic, Dolejskova 3, 18223 Prague, Czech Republic*

Abstract

Electrochemical measurements in aqueous and aprotic media have been carried out on anatase single crystals with exposed (101) and (001) surfaces, respectively. Water reduction and photo-oxidation take place at more negative potentials for the (001) surface than for the (101) surface. This can be rationalized in terms of a more negative flatband potential (by ca. 0.06V) for the (001) face, which is due to dissociative chemisorption of water molecules on this surface. Lithium insertion is favored on the (001) surface, as evidenced by a higher standard rate constant for charge transfer (10^{-8}cm/s vs. $2\cdot10^{-9}$cm/s) and a higher chemical diffusion coefficient for Li^+ insertion ($4\cdot10^{-13}$ cm^2/s vs. $2\cdot10^{-13}cm^2$/s) for the propagation along the c-axis. This can be elucidated by a better structural transparency of the anatase lattice in this direction.

1. Introduction

Since the pioneering study in 1972, titanium dioxide has been recognized as one of the most important electrode materials for semiconductor electrochemistry [1]. Mesoscopic TiO_2 (anatase) electrodes have demonstrated useful properties in photoelectrochemical solar cells [2] and Li-ion batteries [3]. Although these electrodes have already achieved remarkable parameters, fundamental understanding of their properties is still a target of both academic and practical interest. For instance, the relations between the morphology of the anatase surface and its photo/electro/chemical performance is not yet fully elucidated. To rationalize these issues, charge transfer processes should be studied on defined model systems, such as single crystal electrodes.

While the electrochemical properties of rutile single crystals have been studied carefully in the past [1] there are only scarce data about anatase. This has been caused by a lack of reasonably sized and pure anatase crystals (Ref. [1] p. 45). Only recently, we have succeeded in preparing suitable anatase single crystals by a chemical transport reaction [4].

For rutile, the exposed faces are usually (001), (100) or (110), but there are only limited and inconsistent data about the electrochemical properties of different

in press: Journal of the Electrochem. Soc. 1999

faces [1]. Hotsenpiller et al. [5] have recently found pronounced differences in the rates of photocatalytic reactions on various rutile faces.

The rutile electrodes are usually made from commercial crystals grown by Verneuil method. This requires additional surface treatments like polishing and etching, which may introduce defects on the electrode surface. On the other hand, our anatase samples are grown from the gas phase as isolated single crystals exhibiting naturally grown surfaces, for which any polishing and etching can be omitted [4]. To the best of our knowledge, there are no reports about the electrochemical anisotropy of anatase. Hence this is a first paper, which points at salient electrochemical differences between the two naturally available surfaces, i.e. (101) and (001). Besides the usual electrochemical and photoelectrochemical studies in aqueous media, we report also on the effects of Li^+ insertion. This reaction shows interesting relations to the crystallographic structure (rutile/anatase) [6,7] and morphology of polycrystalline electrodes [8,9]. The kinetics of Li^+-insertion should generally depend on the crystallographic orientation of any lithium host: the best example is, presumably, graphite [10]. Similar, although less expressed, anisotropy can be theoretically [11] expected also for anatase. Some of these questions are addressed in the present study.

2. Experimental Section

Anatase single-crystals were grown from the gas phase by a chemical transport reaction as described elsewhere [4]. The transparent and colorless crystals ordinarily have a truncated bipyramidal habitus exhibiting mainly the (101) and (001) surfaces with surface areas between 1 and 4 mm^2. The crystals were then reductively doped by hydrogen at 500-600 °C for 24h. The donor densities (from Mott-Schottky plots, *vide infra*) were between 10^{18} - 10^{20} cm^{-3}. Crystals were contacted by a Ga-In alloy to a copper wire and mounted using TorrSeal (Varian) epoxy resin [4]. The surface orientation of the electrode was proved by X-ray diffraction (Laue camera). Atomic force microscopy (AFM, Topometrix TMX-2010-Discoverer microscope with a pyramidal Si_3N_4 tip) confirmed that the corrugation of the working surfaces was typically below 1 nm. Only in accidental cases, steps or islands up to several hundreds nm were also observed (Fig. 1).

Electrochemical experiments in aqueous solutions were carried out in conventional three-electrode cells using an Autolab (Ecochemie, the Netherlands) potentiostat. The frequencies for the impedance measurements ranged from 100Hz to 1kHz. The reference electrode was a standard Ag/AgCl electrode in saturated KCl solution (Metrohm, Switzerland), a Pt-wire served as the counter electrode. Illumination of the working electrode was accomplished with an Oriel 450W high-pressure xenon lamp through a quartz window in the cell. The light intensity was about 100mW/cm^2 (white light), the distance between cell window and working electrode was approximately 1cm. All potentials in aqueous media are further referred to the Ag/AgCl electrode.

The studies of Li insertion were carried out in a previously optimized [8] solution: 1 M $LiN(CF_3SO_2)_2$ in ethylene carbonate (EC) and 1,2-dimethoxyethane (DME). A 1:1 mixture (by mass) of DC/DME (Aldrich) was dried over a molecular

sieve (Union Carbide 4A). $LiN(CF_3SO_2)_2$ (Fluorad HQ 115 from 3M) was dried at 150°C/1 mPa. The electrolyte solution contained about 10-15 ppm H_2O (Karl Fischer coulometer, Metrohm 684 KF). All operations were carried out in a glove box (Labstar 50, M. Braun, GmbH); the working atmosphere was Ar with typically <1 ppm H_2O and < 1 ppm O_2. Electrochemical data were acquired using a PAR EG&G 263A potentiostat, with anatase working, Pt auxiliary and Li/Li^+ reference electrodes. All potentials in EC/DME solutions are further referred to the Li/Li^+ reference electrode.

To minimize casual spread of experimental data, electrochemical measurements have been carried out with several (usually five) different crystals with either the (101) or (001) orientations, while all other experimental variables (electrolyte composition, temperature, illumination intensity, etc.) were identical. This was best achieved if two crystals were studied simultaneously in the same solution. Since there was always spread in the individual data, we display further representative plots for an experiment producing typical (average) response in a series of parallel measurements on different crystals (Figs. 1-5). However, the graphs displaying "secondary" data (i.e. those calculated from the primary experiments, Figs. 6,7) present all the obtained values.

3. Results and discussion

3.1. Electrochemistry in aqueous media: dark reduction and photo-oxidation of water

In aqueous media, water reduction is usually the dominant process at potentials negative to the flatband, E_{fb}. Fig. 2 displays steady-state cathodic currents of water reduction in 0.5 M HCl at (101) and (001) surfaces, respectively. Both faces show the expected Tafel behavior at higher overvoltages. The charge transfer coefficient equals about 0.3, which is comparable to the values reported for rutile in acidic media [1]. At potentials close to E_{fb}, the cathodic currents diminish, which is better visualized in logarithmic coordinates (Fig. 2). The onset of the water-reduction current appears at -0.22 V vs. Ag/AgCl for the (101) surface and at -0.31 V for the (001) surface. This result points at a less negative flatband potential for the (101) surface.

For a more precise determination of the flatband potential, impedance spectra were recorded. The interfacial capacitance, C fits the Mott-Schottky relation:

$$C^{-2} = 2(E-E_{fb} - kT/e)/e\varepsilon_0\varepsilon_r N \qquad (1)$$

(E is the electrode potential, E_{fb} is the flatband potential, k is the Boltzmann constant, T is the temperature, e is the electron charge, ε_0 is the permittivity of vacuum ε_r is the dielectric constant and N is the donor density). Fig. 3 displays Mott-Schottky plots in 0.5 M HCl for (101) and (001) surfaces, respectively (Figs. 3a, b). Similar plots were obtained also in H_2SO_4 and $HClO_4$ solutions. The dielectric constant of anatase was reported to be 31 for the electric field perpendicular to the a-axes [(001) surface] and 48 for a direction parallel to the a-axes [12]. By using these values, we obtain the average donor densities of 2.5 and $1.2 \cdot 10^{19}$ cm^{-3} for the (101) and the (001) surface,

respectively. The flatband potential is -0.28 ± 0.02 V vs. Ag/AgCl for the (101) face and -0.34 ±0.01 V for the (001) face, respectively.

Fig. 4 displays the photocurrent as a function of applied potential for (101) and (001) surfaces in 0.1 M HCl (Figs. 4a, b). The electrodes were illuminated by chopped white light of a Xe-lamp. The onset of photocurrent is at about -0.28V vs. Ag/AgCl for the (001) orientation and -0.24V for the (101) orientation. The photocurrent raises with the square root of the applied voltage as predicted by the equation [1]:

$$i_{ph}^2 = (2e\varepsilon_0\varepsilon_r I_0^2 \alpha_o^2/N)(E-E_{fb}) \qquad (2)$$

I_0 is the illumination intensity and α_o is the optical absorption coefficient. In contrast to rutile [1,4], we do not observe any saturation photocurrent on anatase at potentials up to ca. 1.5 V vs. E_{fb}. This is a consequence of the smaller dielectric constant of anatase which results in a smaller width of the space charge layer (assuming ε_r for rutile to be 173 [1]). The potential at which the space charge layer is large enough to absorb all photons is therefore shifted up for anatase. The photocurrent raises at slightly more negative potentials for the (001) face, although the difference is only visible after magnification of the critical region of Fig. 4 (see inserts). Apparently recombination effects via surface states attenuate noticeably the photocurrent at potentials close to E_{fb}.

In conclusion, the measurements of (i) dark reduction of water, (ii) photooxidation of water and (iii) interfacial capacitance confirmed, in unison, that the (001) face has more negative E_{fb} as compared to that of the (101) face; the observed shift equals ca. 0.06V±0.02V on the average. In aqueous media, the E_{fb} is controlled by the acid-base equilibrium involving surface OH groups. Recent theoretical calculations [13] indicated a significant difference in the adsorption of water for these two surfaces. The clean (101) surface, which contains half-penta/half-hexacoordinated Ti atoms, adsorbs water non-dissociatively. On the other hand, the clean (001) surface contains only pentacoordinated Ti atoms (cf. also Fig 8 below). On the (001) surface, water is spontaneously dissociated, which leads to the anchoring of isolated OH groups to Ti atoms. All surface Ti atoms stay pentacoordinated even if they carry terminal hydroxyl groups. Consequently, the more acidic (001) surface attracts less protons, which explains the negative shift of E_{fb}.

The demonstrated orientation dependence of the flatband potential may have technological relevance for the anatase-based solar cells. A more negative flatband potential allows higher open circuit photovoltages (OCV) to be achieved in solar cells. Weidmann et al. [14] have found an increase of 30mV in the OCV of dye sensitized solar cells when water was chemisorbed on the anatase films. This shift could be, presumably, increased by the preferential use of (001) surfaces. Such a surface is available, e.g. via self-organization of rod-like particles at controlled conditions [15].

3.2. Electrochemistry in aprotic medium: Li^+ insertion

Fig. 5 displays cyclic voltammograms of anatase (101) and and (001) faces in 1 M $LiN(CF_3SO_2)_2$ + EC/DME. The cathodic/anodic peaks correspond to the insertion/extraction of Li^+ to/from the anatase lattice:

$$TiO_2 + x\,(Li^+ + e^-) \rightarrow Li_xTiO_2 \qquad (3)$$

where the insertion coefficient, x is usually ≤ 0.5 [3,8,16]. The easier Li^+ insertion through the (001) face is clearly apparent, especially at faster scan rates. In contrast to polycrystalline electrodes, which show the ratio of inserted-to-extracted charge [8,16,17] and/or mass [7,18] close to 100 %, the macroscopic single crystals exhibit considerably lower extraction charges as compared to those for insertion. This is apparently caused by the diffusion of Li^+ into the bulk crystal, from where the Li^+ ions are not completely recuperated at time base of the reverse scan.

The voltammograms in Fig. 5 confirm that the charge transfer processes follow irreversible kinetics. Consequently, the charge transfer coefficients, α can be calculated from the equation [19]:

$$\alpha = 1.857RT/nF(E_p - E_{p/2}) \qquad (4)$$

where n is the number of electrons in the rate-determining step, E_p is the peak potential, $E_{p/2}$ is the half-peak potential and the other symbols have their usual meaning. At slower scans, the charge transfer coefficients equal about 0.3 - 0.4 for insertion and 0.6-0.7 for extraction, which matches the values reported for polycrystalline electrodes [16].

The standard rate constant of charge-transfer, k_0 can be estimated from the peak current density i_p by applying the equation [19]:

$$i_p = 0.227nFck_0 \exp[-\alpha nF(E_p - E_0')/RT] \qquad (5)$$

where E_0' is the formal potential estimated from the center between the peak potentials for the slowest scan and c is the maximum concentration of Li^+ (or Ti^{3+}) in the accumulation layer. Assuming the limiting composition of the insertion product to be $Li_{0.5}TiO_2$ (cf. Eq. 3) [8,16,17], the concentration c equals 0.024 mol/cm^3. Fig. 6 displays the corresponding plots for Li^+ insertion into the two different anatase faces. The data were obtained for ten different crystals (five crystals per each orientation) and scan rates between 1 and 0.02 mV/s. By fitting the data in Fig. 6 to Eq. 5, the charge transfer coefficients equal 0.3 or 0.2 for (101) or (001) faces, respectively, and the standard rate constants for Li^+ insertion equal $2\cdot10^{-9}$ cm/s or 10^{-8} cm/s for (101) or (001) faces, respectively.

The peak current density at a given scan rate, v is also related to the chemical diffusion coefficient of Li^+ in the anatase lattice, D [19]:

$$i_p = 0.4958nFc\,(D\alpha nFv/RT)^{1/2} \qquad (6)$$

By using analogous evaluation routine for ten different crystals, we obtained the average diffusion coefficients for Li^+ insertion equal to $(7\pm2)\cdot10^{-14}$ cm^2/s or $(2.0\pm0.8)\cdot10^{-13}$ cm^2/s for the (101) or (001) orientation, respectively.

Further insight into the rate of Li^+ transport in anatase can be obtained by using potential-step chronoamperometry [8,17,20]. The applied potential steps were from 3 V to the insertion potential (whose values were changed between 1.5 to 1.1 V) and back to 3 V; the registration times were between 200 s and 20 ks. In contrast to polycrystalline anatase electrodes [17], the chronoamperometric current densities, i_{ch} on single crystal electrodes obey formally the Cottrell equation in a broad interval of potentials and times, t [4]:

$$i_{ch} = FD^{1/2}c\pi^{-1/2}t^{1/2} \qquad (7)$$

c is concentration (as in Eq. 5) and D is chemical diffusion coefficient. The experimental curves (not shown here, but similar to those in Fig. 8, in Ref. [4]) gave reproducible D values, especially at insertion potentials $\approx<$ 1.3 V.

Fig. 7 displays the chronoamperometric diffusion coefficients (Eq. 7) of Li^+ insertion (Fig. 7a) and extraction (Fig. 7b) measured at various temperatures (from 23 to 58 °C) with different crystals. At 25 °C, the values for insertion are $2\cdot10^{-13}$ cm^2/s or $4\cdot10^{-13}$ cm^2/s for the (101) or (001) faces, respectively (Fig. 7a). The corresponding values for extraction at 25 °C, are $6\cdot10^{-13}$ cm^2/s or 10^{-12} cm^2/s, respectively (Fig. 7b). The chronoamperometric diffusion coefficients for Li^+ insertion are by a factor of 2-3 higher than those calculated from voltammetric data (see above). Interestingly, the same shift is apparent, if we compare the literature data from chronoamperometric [20] and voltammetric [16] measurements on polycrystalline anatase.

The diffusion coefficients follow an Arrhenius-type temperature dependence:

$$D = D_0 \exp(-E_a/kT) \qquad (8)$$

where E_a is the activation energy. From Fig. 7 and Eq. (8), we can estimate the activation energies for Li^+ insertion to be between 0.6-0.7 eV and for extraction about 0.5 eV for both orientations of the anatase crystal. These values are in a remarkable agreement with the activation energy predicted theoretically by ab-initio calculations, (E_a = 0.6 eV) [11] and also with the values reported for polycrystalline anatase (0.51-0.66) [11,21].

Both voltammetric and chronoamperometric experiments point at more facile Li^+ insertion through the (001) face. This fits theoretical predictions that Li^+ in anatase moves along zigzag channels connecting the octahedral voids in the lattice, i.e. the positions (0.52 0.50, 0.02) and (0.50, 1.01, 0.25) [11]. Fig. 8 shows that these paths are roughly perpendicular to the (001) face. Some authors [1,21] have also considered a straight transport along the a-axes, i.e. between the positions (0.52, 1.50, 0.02) and (0.50, 1.01, 0.25) which would, reportedly, require even lower activation energies (0.37-0.46 eV) [21]. However, this prediction [21] was later retracted by the same group [11], and we consider, therefore, that Li^+ moves solely along the zigzag pathways shown in Fig. 8.

The transport of Li^+ to a certain distance perpendicular to the (001) face requires less jumps between the equilibrium positions than the same excursion underneath the (101) face. From Fig. 8, the effective diffusion distances per one jump equal 189 pm, 205 pm or 238 pm for the directions perpendicular to the (100), (101) or (001) faces, respectively. Hence, the faster diffusion through the (001) face is supported also by simple geometric arguments.

The conclusion that the (001) face is more permeable for Li^+ also rationalizes our previous experimental finding that rod-like self-organized anatase nanocrystals show more facile accommodation of Li^+ as compared to ordinary, statistically oriented nanocrystals [9]. The surface of an array of self-organized particles (rods) is composed of (001) faces [15], i.e. it is a mosaic structure, which mimics the (001) face of a single crystal. On the other hand, the ordinary and non-oriented crystals expose prevailingly their (101) faces. This finding may also have straightforward practical implications for anatase-based lithium batteries [3].

4. Conclusions

Our results show clearly an orientation dependence of charge transfer processes on anatase electrodes. In aqueous solutions, the (101) and the (001) surface have different flatband potentials due to different chemisorption of water on the anatase *surface*. This gives rise to a negative shift of the onset potential for dark reduction and photo-oxidation of water for the (001) surface. In aprotic solvents, differences in the insertion of lithium ions are also due to the anisotropy of the tetragonal *bulk* anatase lattice, which is less dense in the (001) planes as compared to the (101) planes. Therefore, the propagation of Li^+ into anatase is faster in the c-axis direction. The demonstrated orientational effects on the charge transfer on single crystals may have some technological relevance for the mesoscopic films used in the solar cells and lithium batteries.

Acknowledgment

This work was supported by the Swiss National Science Foundation (contract No. 2100/046825.96/1) and by the Academy of Sciences of the Czech Republic (contract No. A4040804). Thanks are due to Dr. K. Schenk from the crystallographic institute of the University of Lausanne for Laue measurements and Dr. Pavel Janda from the Heyrovsky Institute, Prague for AFM measurements.

Figure captions

Fig. 1 (a) AFM pattern of a (101) surface of anatase single crystal; scanned area 0.5 · 0.5 μm^2 (b) AFM pattern of a (101) surface of anatase single crystal; scanned area 5.51 · 5.51 μm^2. The picture 1b shows an occasionally detected island, ca. 100 nm in height.

Fig. 2 Steady state currents of water reduction. Full line: (001) surface. Dashed line: (101) face.

Fig. 3 Mott-Schottky plots of the (101) surface (Fig 3a) and the (001) surface (Fig 3b) of anatase. The frequencies of the ac currents were 315Hz, 395Hz, 450Hz, 525Hz, 630Hz, 788Hz and 1051Hz, from the lowest to the highest curve, respectively.

Fig. 4 Photocurrent densities for the (101) surface (Fig 3a) and the (001) surface (Fig 3b) of anatase single crystal. The inserts show a magnification of the region where the photocurrent starts. The electrode was illuminated with a white light (0.1 W/cm^2) of a high-pressure Xe lamp.

Fig. 5 Typical cyclic voltammogram of single crystal anatase in 1 M $LiN(CF_3SO_2)_2$ + EC/DME (1:1 by mass). Full line: the (001) face exposed. Dashed line: the (101) face exposed. The scan rate is 0.5 mV/s (Fig. 5a) or 0.1 mV/s (Fig. 5b).

Fig. 6 Voltammetric peak current densities vs. the potential difference plotted according to Eq. 5. Full line, full points the (001) face exposed. Dashed line, open points: the (101) face exposed. Different crystals are distinguished by different point markers.

Fig. 7 Chemical diffusion coefficients for Li^+ insertion (Fig. 7a) or extraction (Fig. 7b) calculated from chronoamperometric data. Full line, full points the (001) face exposed. Dashed line, open points: the (101) face exposed. Different crystals are distinguished by different point markers.

Fig. 8 Scheme of anatase lattice with the insertion pathways between octahedral interstitial voids (black full lines). Large gray spheres: oxygen, small gray spheres: titanium, small black spheres: lithium.

Reference List

1. H.O. Finklea, in *Semiconductor Electrodes,* H.O. Finklea, Editor, pp. 44-145, Elsevier, Amsterdam (1988).

2. B. O`Regan and M. Grätzel, *Nature.*, **353,** 737 (1991).

3. S.Y. Huang, L. Kavan, M. Grätzel and I. Exnar, *J.Electrochem.Soc.*, **142,** 142 (1995).

4. L. Kavan, M. Grätzel, S.E. Gilbert, C. Klemenz and H.J. Scheel, *J.Am.Chem.Soc.*, **118,** 6716 (1996).

5. P.A.M. Hotsenpiller, J.D. Bolt, W.E. Farneth, J.B. Lowekamp and G.S. Rohrer, *J.Phys.Chem.B.*, **102,** 3216 (1999).

6. A. Stashans, S. Lunell, R. Bergström, A. Hagfeldt and S.E. Lindquist, *Phys.Rev.B.*, **53,** 159 (1996).

7. L. Kavan, D. Fattachova and P. Krtil, *J.Electrochem.Soc.*, **146,** 1375 (1999).

8. L. Kavan, M. Grätzel, J. Rathousky and A. Zukal, *J.Electrochem.Soc.*, **143,** 394 (1996).

9. P. Krtil, D. Fattachova, L. Kavan, S.D. Burnside and M. Grätzel, *Solid State Ionics.*, in press.

10. T. Tran and K. Kinoshita, *J.Electroanal.Chem.*, **386,** 221 (1995).

11. S. Lunell, A. Stashans, H. Lindström and A. Hagfeldt, *J.Am.Chem.Soc.*, **119,** 7374 (1997).

12. H. Tang, *Electronic Properties of Anatase TiO2 Investigated by Electrical and Optical Measurements on Single Crystals and Thin Films,* EPFL, Thése No. 1311, Lausanne (1995).

13. A. Vittadini, A. Selloni, F. Rotzinger and M. Grätzel, *Phys.Rev.Lett.*, **81,** 2954 (1998).

14. J. Weidmann, T. Dittrich, I. Lauermann, I. Uhlendorf and F. Koch, *Solar Energy Mat.Sol.Cells.*, **56,** 153 (1999).

15. S.D. Burnside, V. Shklover, C. Barbe, P. Comte, F. Arendse, K. Brooks and M. Grätzel, *Chem.Mater.*, **10,** 2419 (1998).

16. H. Lindström, S. Södergen, A. Solbrand, H. Rensmo, J. Hjelm, A. Hagfeldt, and S.E. Lindquist, *J.Phys.Chem.B.*, **101,** 7717 (1997).

17. L. Kavan, K. Kratochvilová and M. Grätzel, *J.Electroanal.Chem.*, **394,** 93 (1995).

18. P. Krtil, L. Kavan and D. Fattachova, *J.Solid State Elctrochem.*, **1**, 83 (1997).

19. A.J. Bard and L.R. Faulkner, *Electrochemical Methods Fundamnetlas and Applications*, J. Wiley & Sons, New York (1980).

20. H. Lindström, S. Södergen, A. Solbrand, H. Rensmo, J. Hjelm, A. Hagfeldt and S.E. Lindquist, *J.Phys.Chem.B.*, **101**, 7710 (1997).

21. M. Stromme Matttsson, M. Veszelei, G.A. Niklasson, C.G. Granqvist, A. Stashans and S. Lunell, in *Electrochromic Materials III*, K.C. Ho, C.B. Greenberg, and D.M. McArthur, Editors, pp. 229-243, The Electrochemical Society, Inc., Pennington (1997).

1 (a)

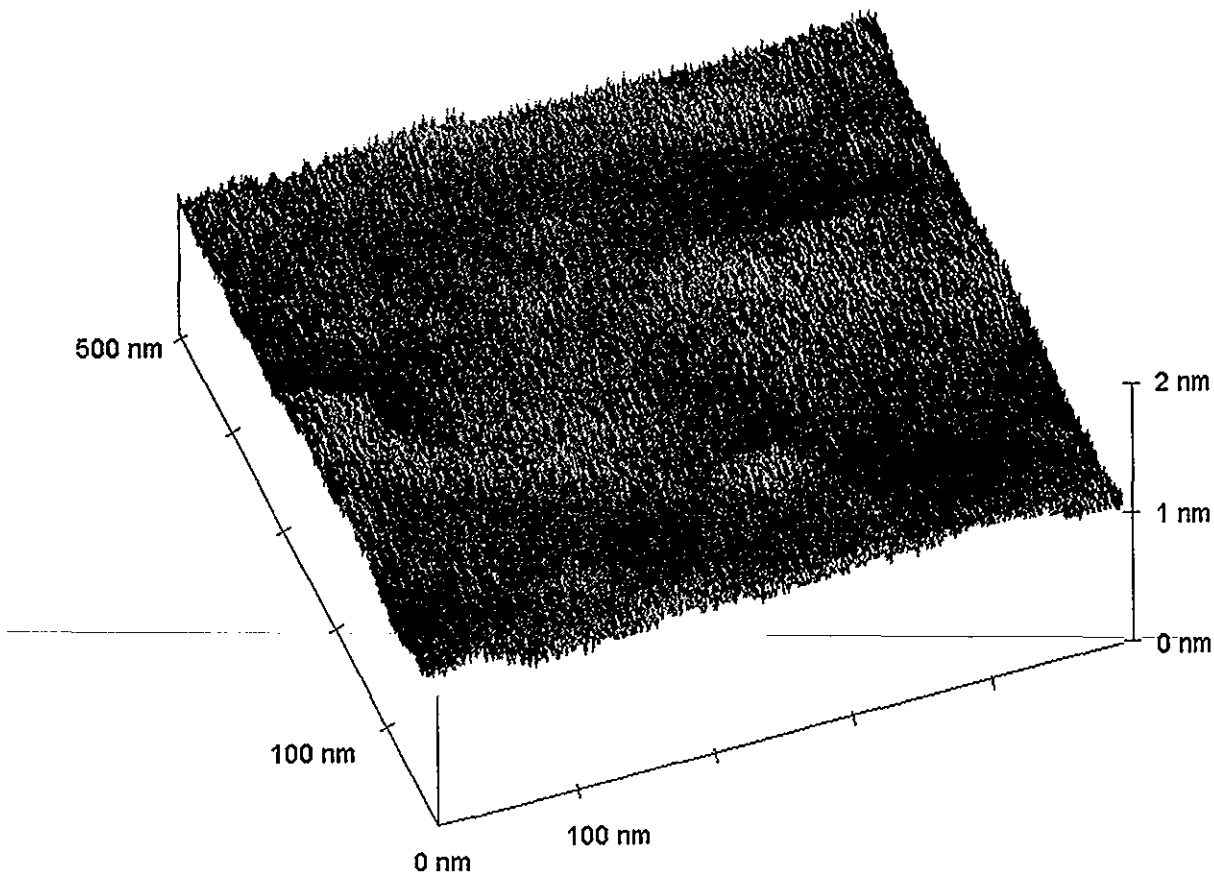

1(b)

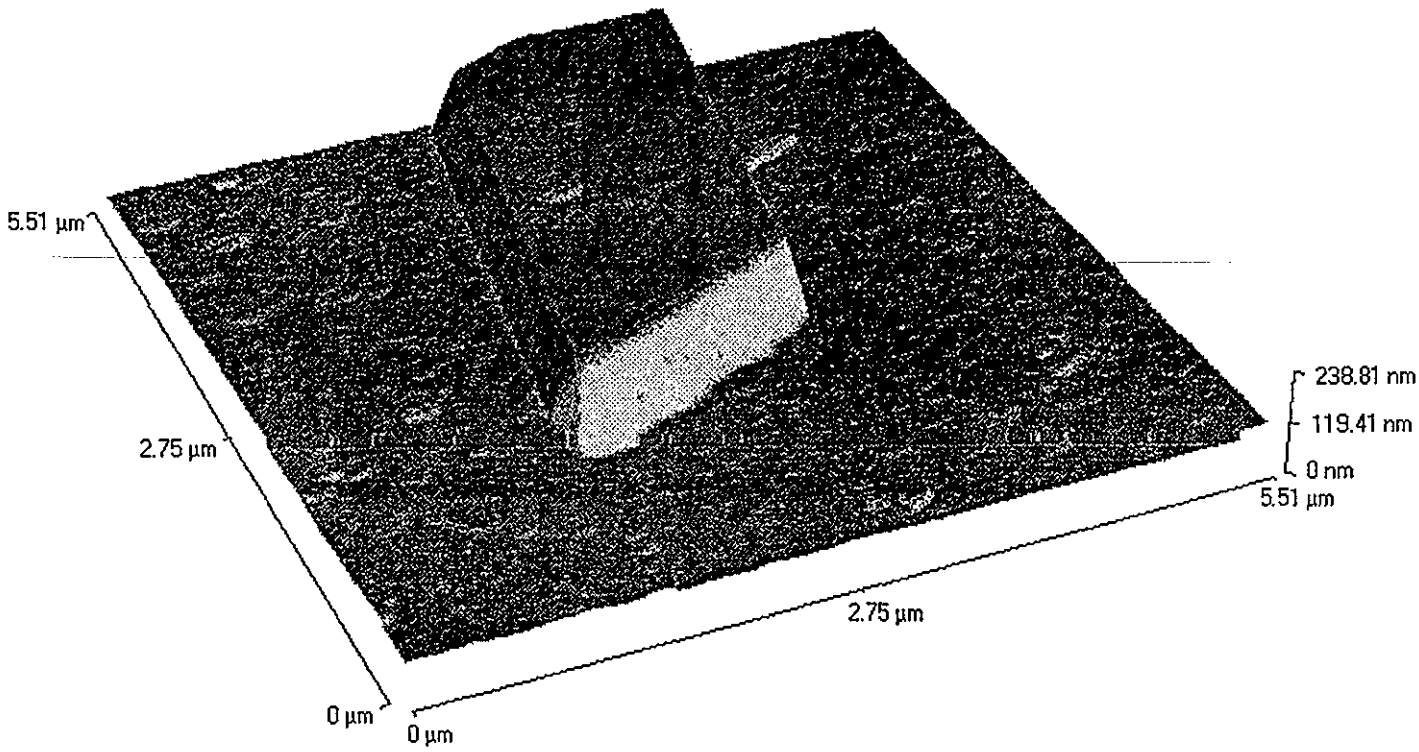

2)

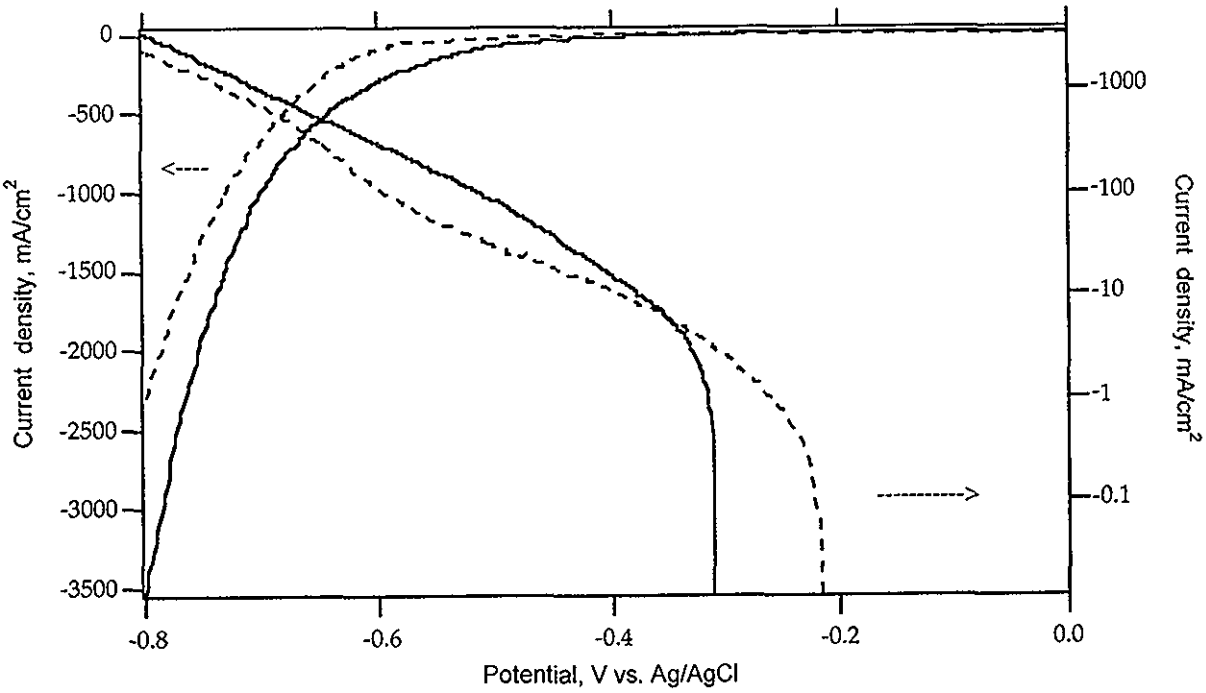
0
-500
-1000
-1500
-2000
-2500
-3000
-3500
Current density, mA/cm2
<----
-1000
-100
-10
-1
-0.1
Current density, mA/cm2
---------->
-0.8
-0.6
-0.4
-0.2
0.0
Potential, V vs. Ag/AgCl

3(a)

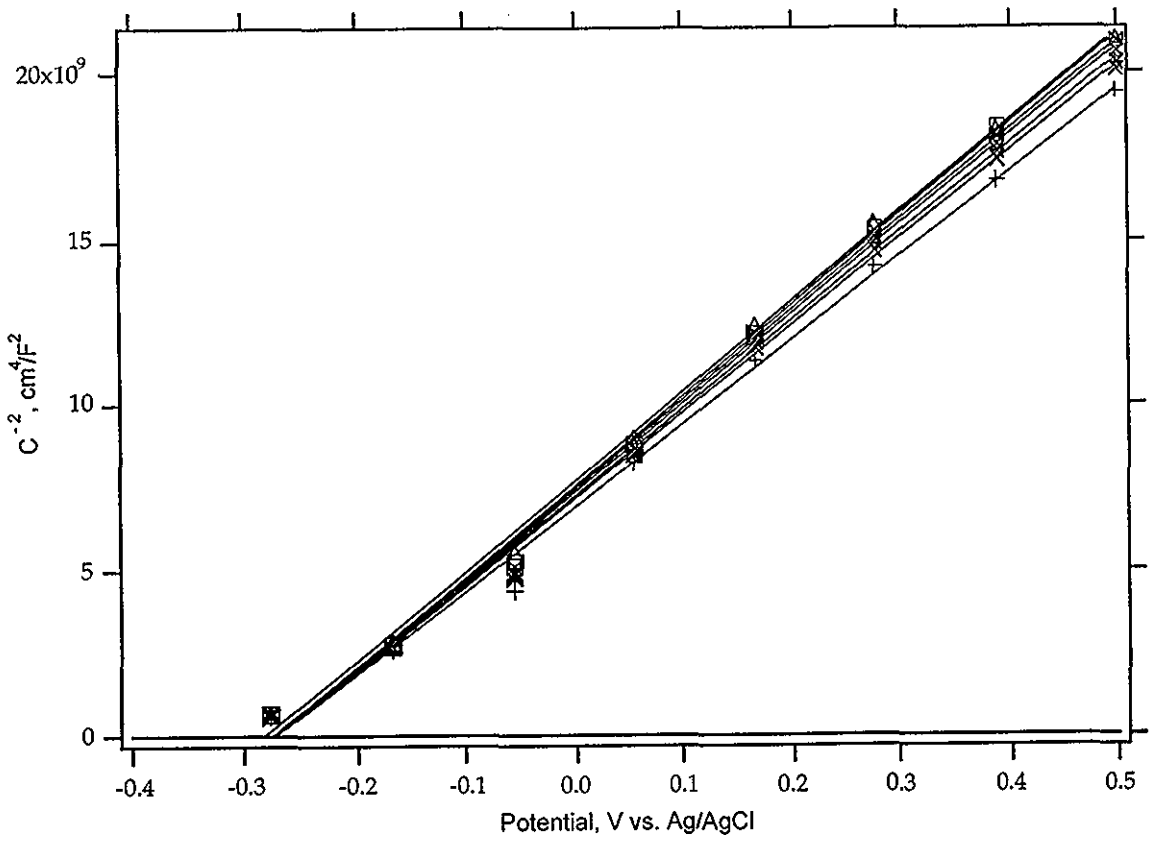
20x10^9
15
10
5
0
C^-2, cm^4/F^2
-0.4
-0.3
-0.2
-0.1
0.0
0.1
0.2
0.3
0.4
0.5
Potential, V vs. Ag/AgCl

3 (b)

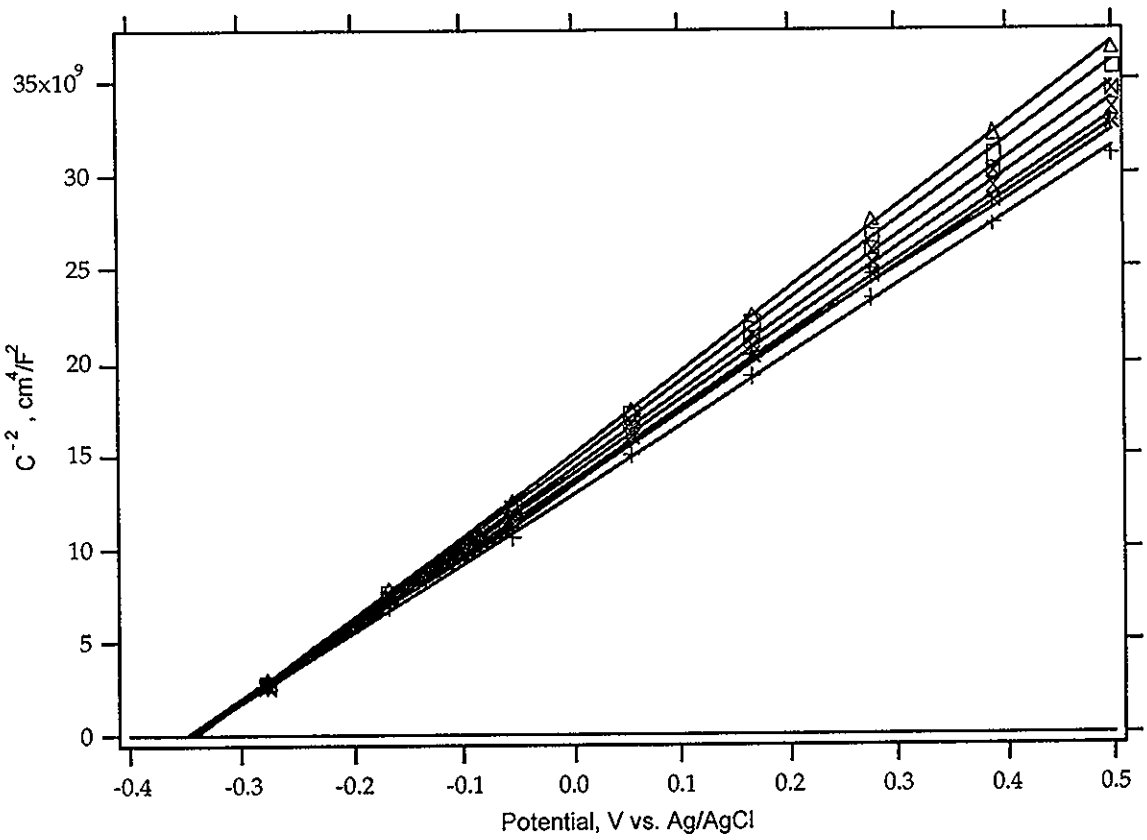
35x10^9
30
25
20
15
10
5
0
C^-2, cm^4/F^2
-0.4
-0.3
-0.2
-0.1
0.0
0.1
0.2
0.3
0.4
0.5
Potential, V vs. Ag/AgCl

4 (a)

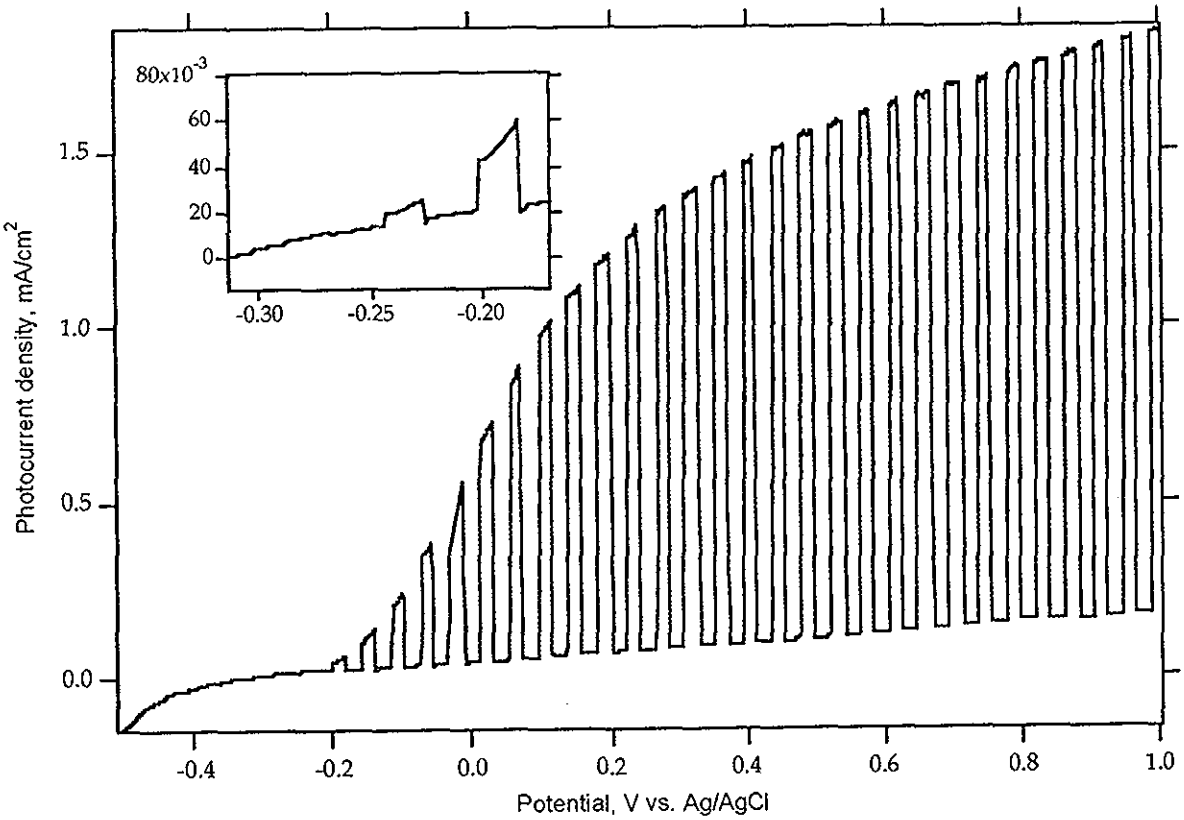
80x10-3
60
40
20
0
-0.30
-0.25
-0.20
1.5
1.0
0.5
0.0
Photocurrent density, mA/cm2
-0.4
-0.2
0.0
0.2
0.4
0.6
0.8
1.0
Potential, V vs. Ag/AgCl

4(b)

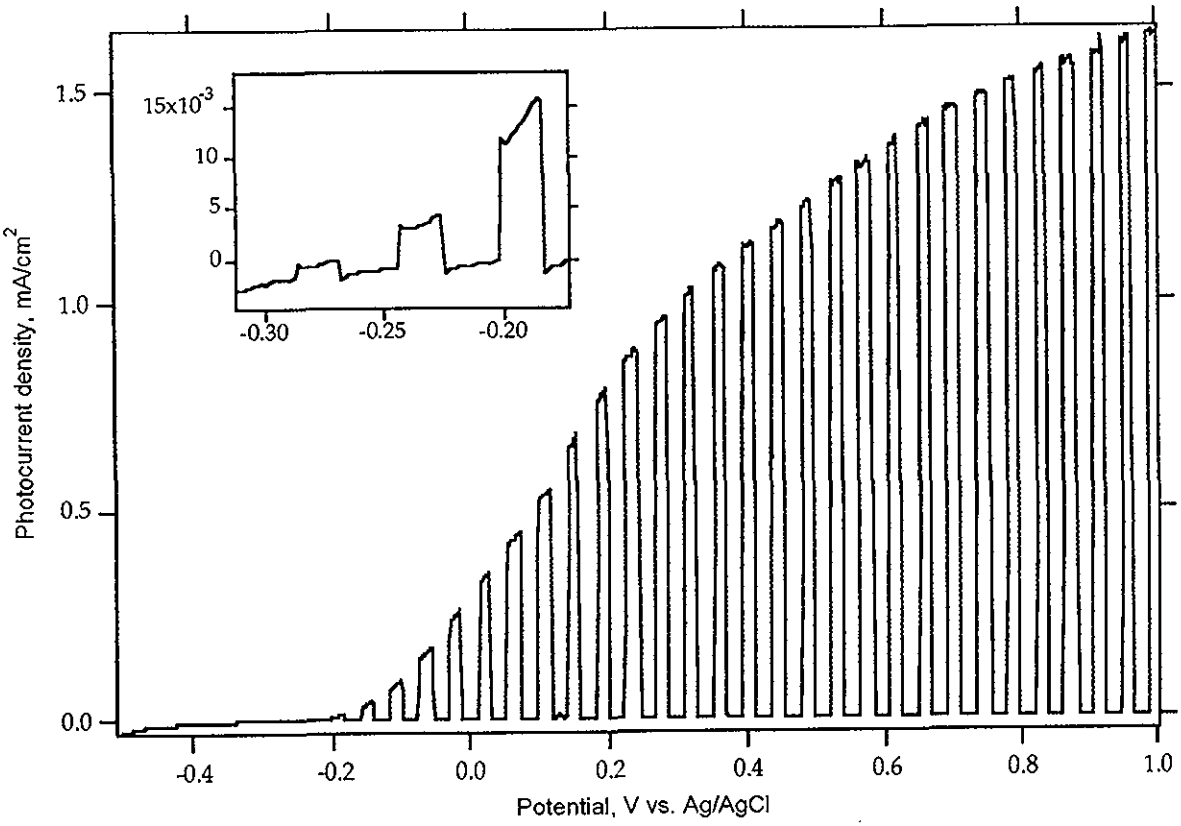
15x10-3
10
5
0
-0.30
-0.25
-0.20
1.5
1.0
0.5
0.0
Photocurrent density, mA/cm2
-0.4
-0.2
0.0
0.2
0.4
0.6
0.8
1.0
Potential, V vs. Ag/AgCl

5. (a)

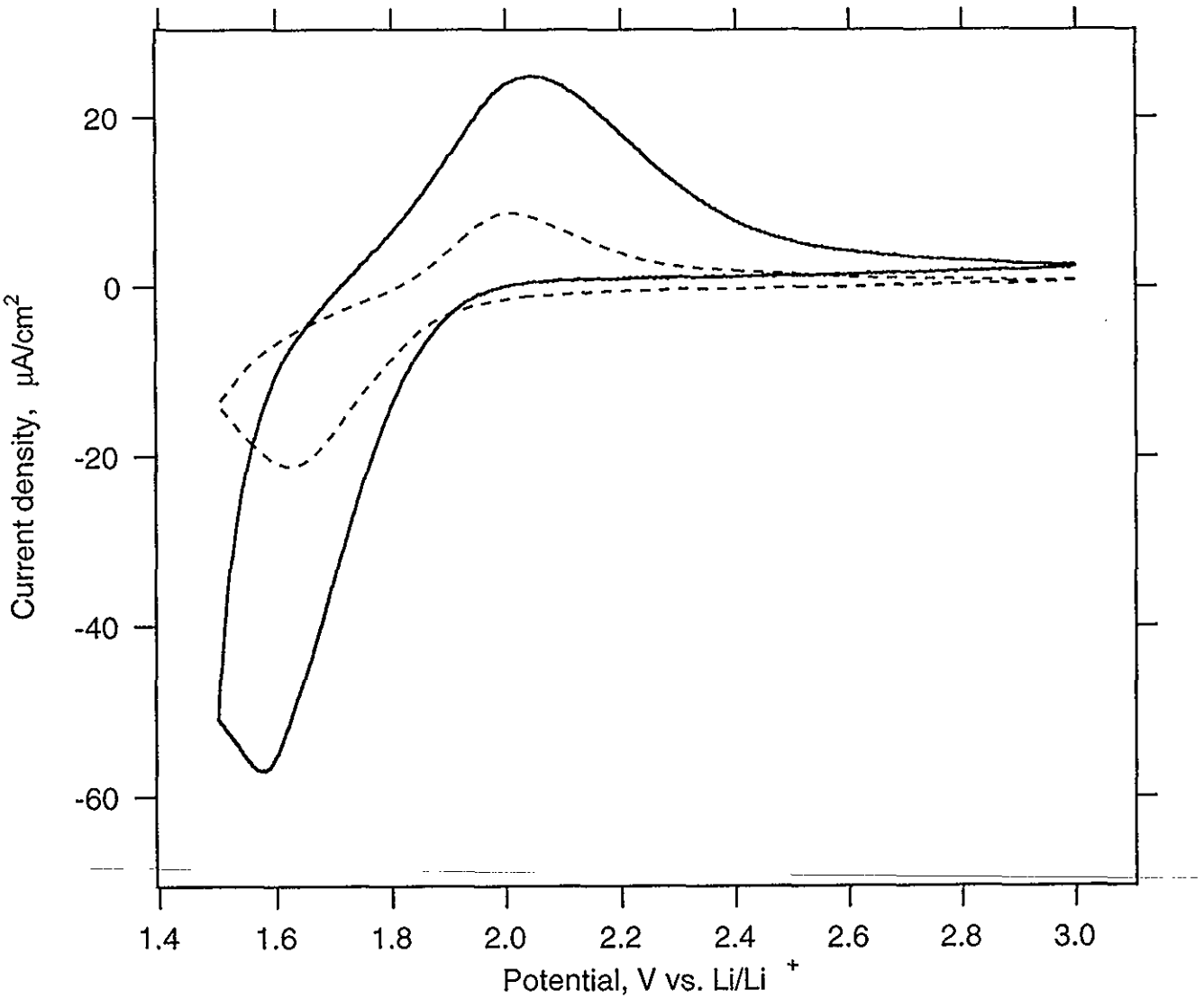
20
0
-20
-40
-60
Current density, μA/cm2
1.4
1.6
1.8
2.0
2.2
2.4
2.6
2.8
3.0
Potential, V vs. Li/Li +

5 (5)

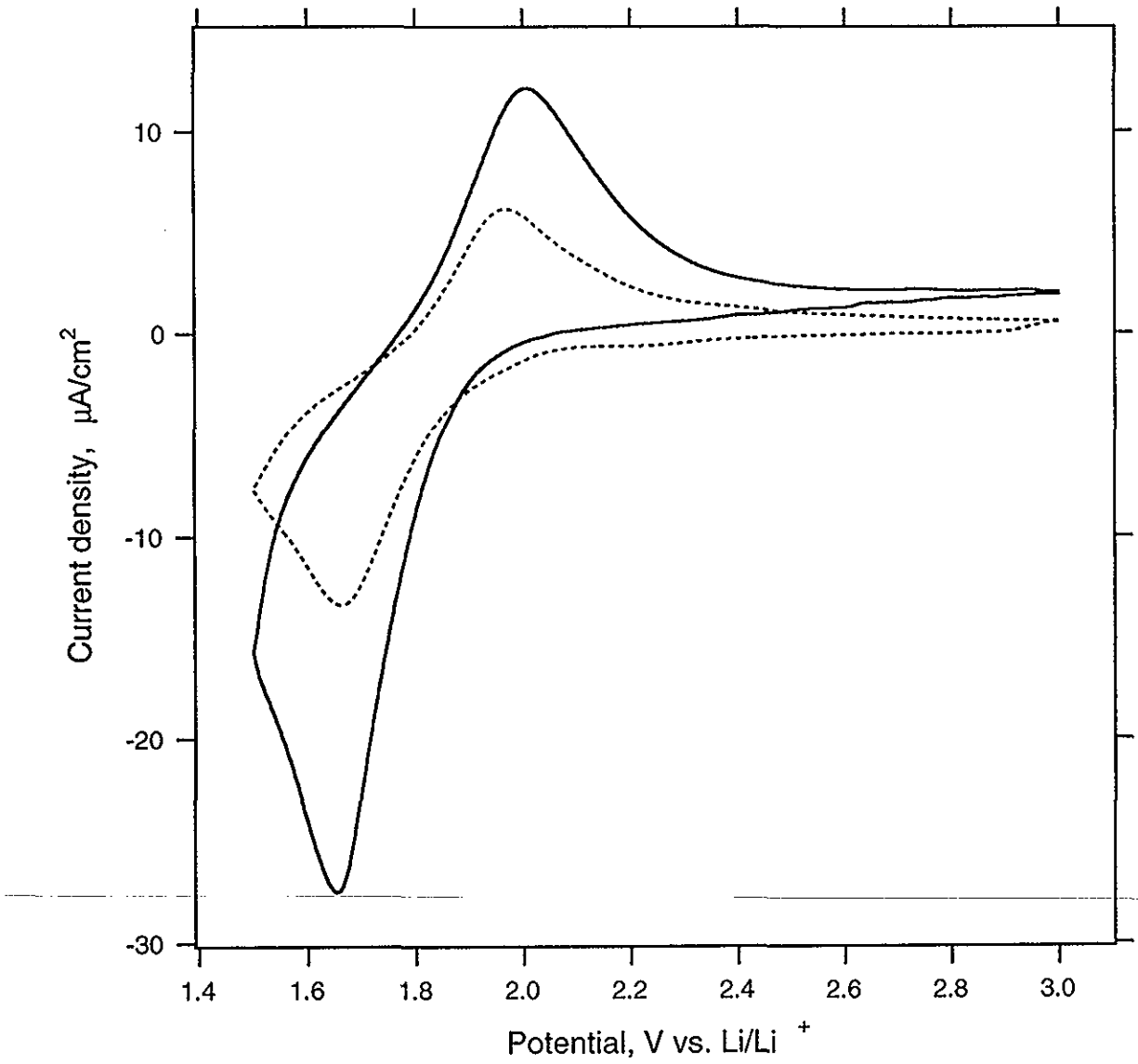
10
0
-10
-20
-30
Current density, μA/cm2
1.4
1.6
1.8
2.0
2.2
2.4
2.6
2.8
3.0
Potential, V vs. Li/Li +

6)

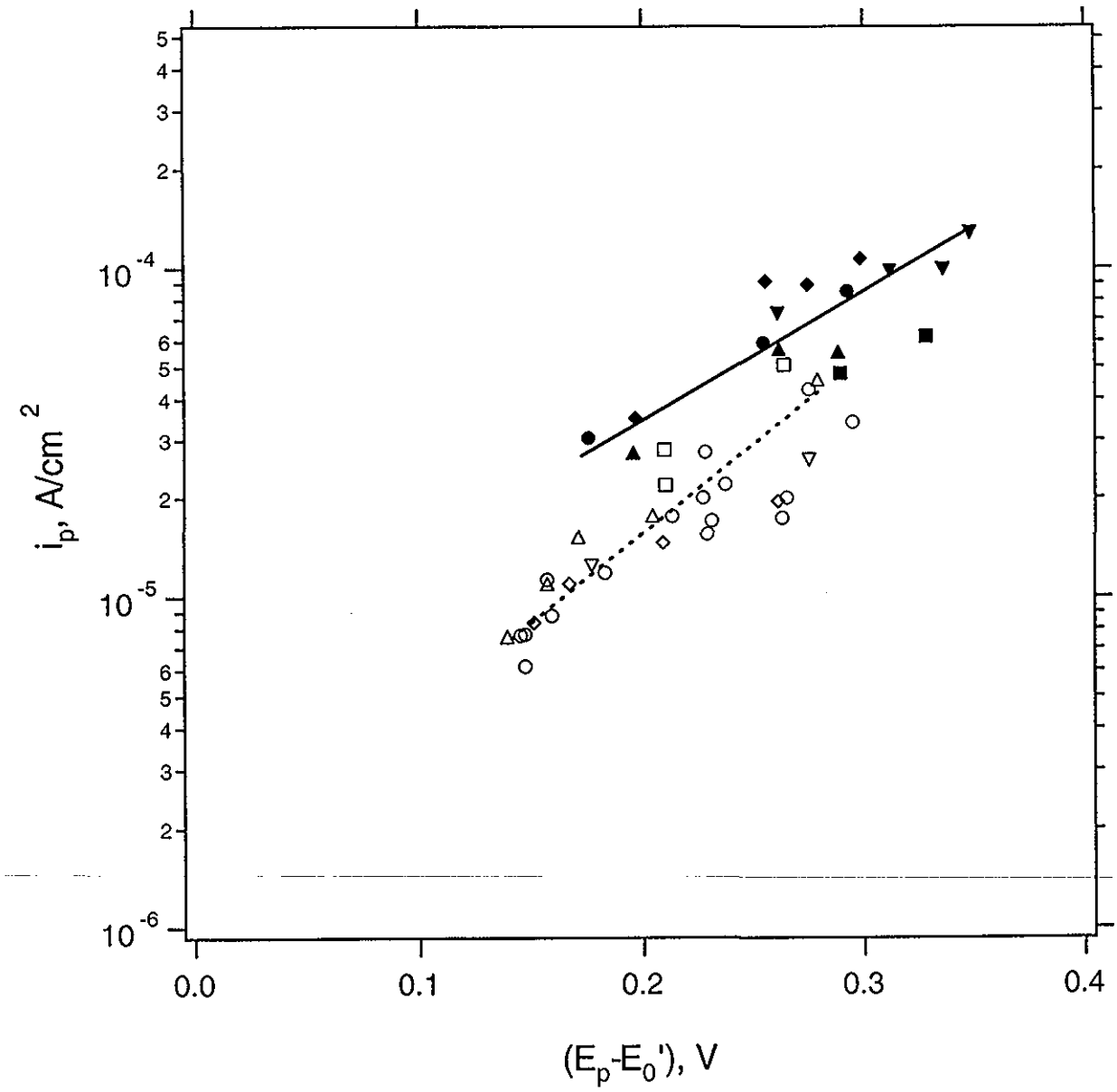

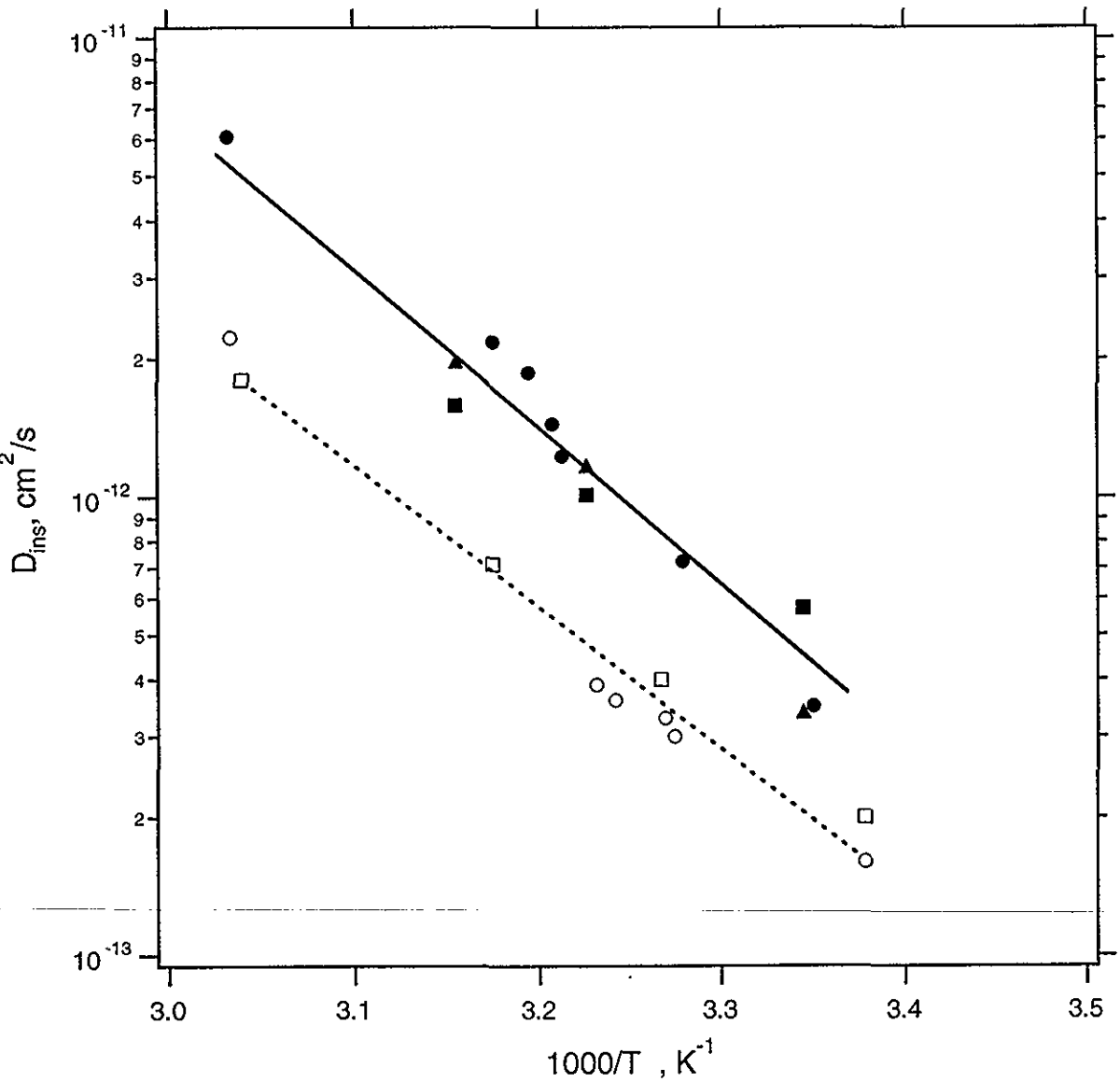
10^{-11}
10^{-12}
10^{-13}
D_{ins}, cm^2/s
3.0
3.1
3.2
3.3
3.4
3.5
1000/T , K^{-1}

7(5)

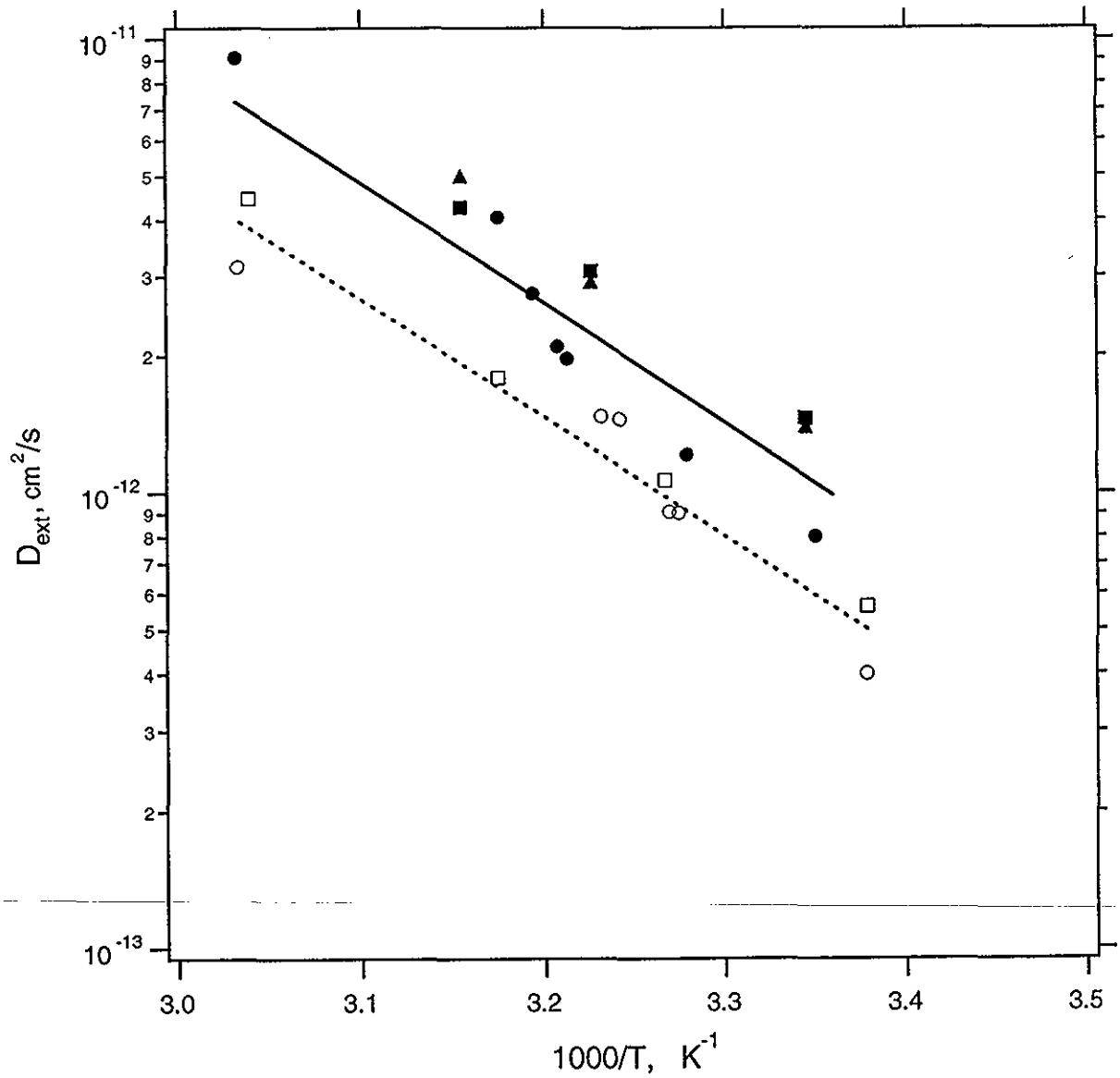

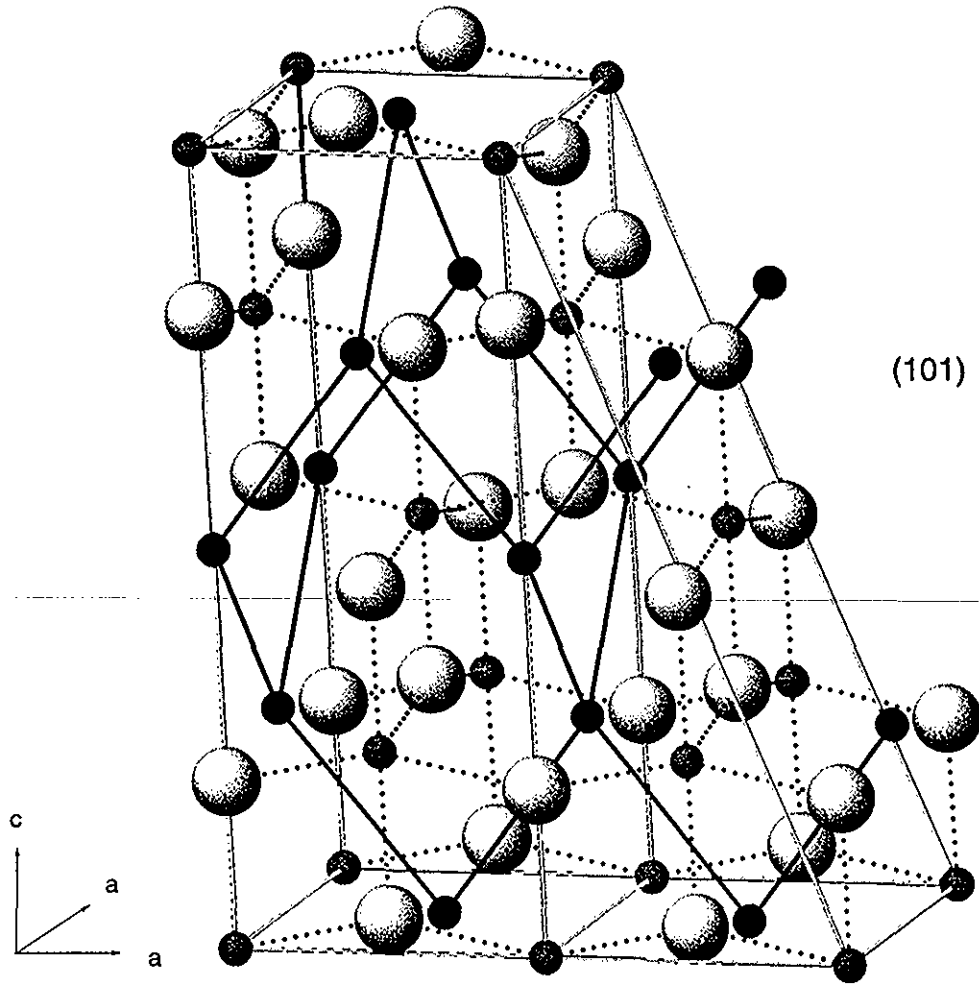
(001)
(101)
c
a
a